

Misalignment between cold gas and stellar components in early-type galaxies

O. Ivy Wong,^{1*} K. Schawinski,² G.I.G. Józsa,^{3,4,5} C.M. Urry,^{6,7} C.J. Lintott,⁸
B.D. Simmons,⁸ S. Kaviraj,^{8,9} and K.L. Masters^{10,11}

¹ *International Centre for Radio Astronomy Research, The University of Western Australia M468, 35 Stirling Highway, Crawley, WA 6009, Australia*

² *Institute for Astronomy, ETH Zurich, Wolfgang-Pauli-Strasse 27, 8093 Zürich, Switzerland*

³ *SKA South Africa, Radio Astronomy Research Group, 3rd Floor, The Park, Park Road, Pinelands, 7405, South Africa*

⁴ *Rhodes University, Department of Physics and Electronics, Rhodes Centre for Radio Astronomy Techniques & Technologies, P.O. Box 94, Grahamstown 6140, South Africa*

⁵ *Argelander Institut für Astronomie (AlfA), University of Bonn, Auf dem Hügel 71, 53121 Bonn, Germany*

⁶ *Yale Center for Astronomy and Astrophysics and Department of Physics, Yale University, P.O. Box 208120, New Haven, CT 06520-8120, USA*

⁷ *Department of Astronomy, Yale University, P.O. Box 208101, New Haven, CT 06520-8101, USA*

⁸ *Oxford Astrophysics, Denys Wilkinson Building, Keble Road, Oxford OX1 3RH, UK*

⁹ *Centre for Astrophysics Research, University of Hertfordshire, College Lane, Hatfield, Herts, AL10 9AB, UK*

¹⁰ *Institute of Cosmology & Gravitation, University of Portsmouth, Dennis Sciama Building, Portsmouth, PO1 3FX, UK*

¹¹ *South East Physics Network (SEPN), www.sepnet.ac.uk*

Released 2011 Xxxxx XX

ABSTRACT

Recent work suggests blue ellipticals form in mergers and migrate quickly from the blue cloud of star-forming galaxies to the red sequence of passively evolving galaxies, perhaps as a result of black hole feedback. Such rapid reddening of stellar populations implies that large gas reservoirs in the pre-merger star-forming pair must be depleted on short time scales. Here we present pilot observations of atomic hydrogen gas in four blue early-type galaxies that reveal increasing spatial offsets between the gas reservoirs and the stellar components of the galaxies, with advancing post-starburst age. Emission line spectra show associated nuclear activity in two of the merged galaxies, and in one case radio lobes aligned with the displaced gas reservoir. These early results suggest that a kinetic process (possibly feedback from black hole activity) is driving the quick truncation of star formation in these systems, rather than a simple exhaustion of gas supply.

Key words: galaxies: elliptical and lenticular, cD, galaxies: evolution, galaxies: formation

1 INTRODUCTION

Star-forming galaxies show a correlation between stellar mass and star formation rate whose normalisation varies with redshift, but whose scatter remains tight out to high redshift (Noeske et al. 2007; Peng et al. 2010; Elbaz et al. 2011). This correlation can be explained as a balance between gas inflows from cosmological scales and outflows driven by supernovae (Bouché et al. 2010; Lilly et al. 2013). Quenching of star formation causes galaxies to depart from this steady-state along pathways that depend on the evolution of the gas supply and reservoir (Schawinski et al. 2014): if the cosmological gas supply to a galaxy is shut off, it will

slowly exhaust its gas reservoir by forming stars at a declining rate. If instead the gas reservoir fuelling star formation is destroyed effectively instantaneously, then star formation will cease and the galaxy will redden rapidly within 1 Gyr, as is observed in early-type galaxies (ETGs; Kaviraj et al. 2011; Wong et al. 2012; Schawinski et al. 2014). Interestingly, this timescale of 1 Gyr is consistent with that proposed for the transition of a merger-driven Ultraluminous Infrared Galaxy (ULIRG) to an ETG (Emonts et al. 2006). Also, it has been known for a while that ULIRGs have a high merger fraction (Sanders et al. 1988).

In addition, negative feedback from a galaxy’s central active galactic nuclei has often been invoked in galaxy formation models to slow down the star formation history of simulated galaxies (e.g. Croton et al. 2006). However,

* E-mail:ivy.wong@uwa.edu.au

[h]

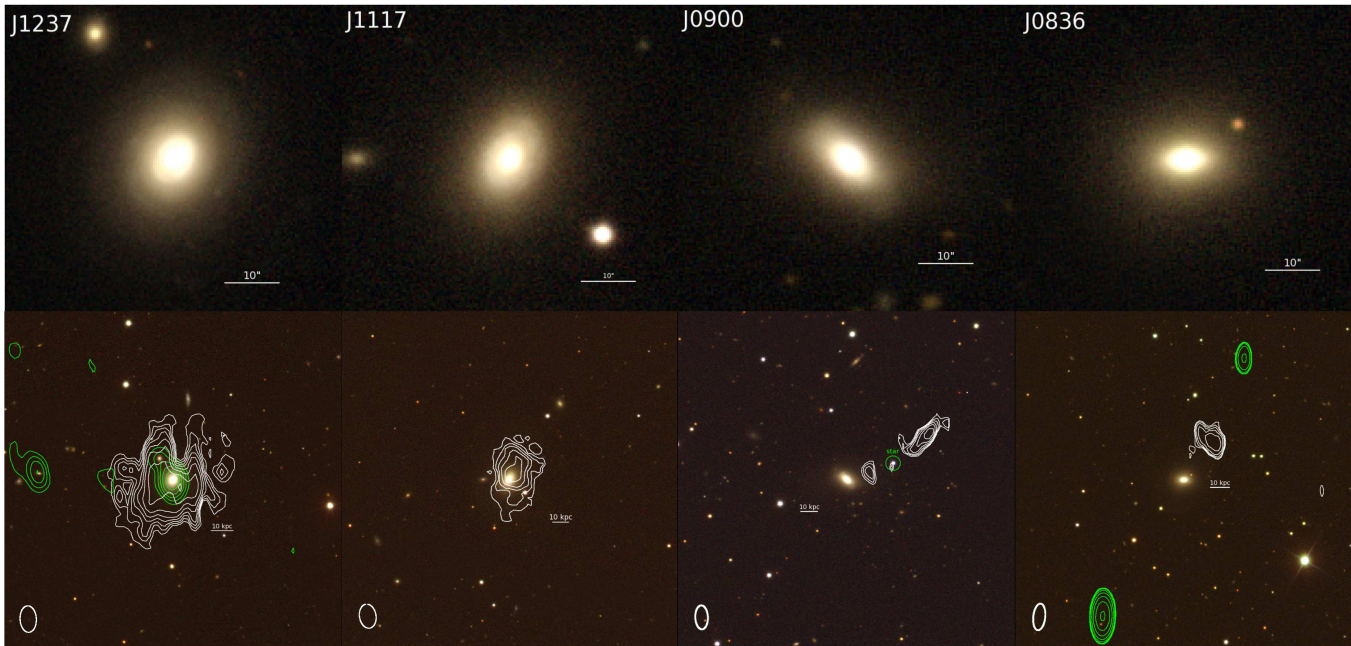


Figure 1. Top row: optical *gri* SDSS (Ahn et al. 2014) composite images of the four blue early-type galaxies in our sample. The galaxies are arranged from left to right in terms of $NUV - u$ colour from blue to red as a tracer of time. The white scale bars represent 10 arcseconds. Bottom row: zoomed-out optical images with the WSRT radio observations overlaid. The white contours (asinh-stretch) represent the HI and the green contours (logarithmic stretch) the radio continuum. The lowest radio and HI contours begin at 3σ and the highest contour is matched to the peak flux density of $0.87 \text{ mJy beam}^{-1}$, $1.51 \text{ mJy beam}^{-1}$, $0.86 \text{ mJy beam}^{-1}$, $44.79 \text{ mJy beam}^{-1}$ for J1237, J1117, J0900 and J0836; respectively. It should be noted that the nuclear 1.4 GHz continuum point sources are not shown for J0900 and J1117 to avoid confusion with the HI contours.

observational evidence for such feedback is currently only available for a few individual galaxies (Harrison et al. 2014; Nyland et al. 2013; Alatalo et al. 2011; Hota et al. 2011; Croston et al. 2008; Kharb et al. 2006). With the advent of very large surveys; much progress has been made towards understanding of the co-evolution between galaxies and their central AGN, in particular, the connection between classical bulges and central supermassive black holes (Heckman & Best 2014; Kormendy & Ho 2013).

Blue ETGs do not fit the canonical bimodal scheme of red ellipticals versus blue spirals and are unlikely to be the descendants of blue spirals (Tojeiro et al. 2013). Rather, the blue ETGs appear to be transition-type galaxies and are probable predecessors of local post-starburst galaxies (Schawinski et al. 2009; Wong et al. 2012). Previous CO observations of blue ETGs show that the molecular gas reservoirs are being rapidly destroyed during the composite star formation and AGN phase (Schawinski et al. 2009). Local post-starburst galaxies are defined to be galaxies which have recently ceased forming stars. These galaxies typically show little $H\alpha$ or $[OII]$ emission (indicative of current star formation), but have strong absorption line signatures indicative of a young stellar population. In addition, local post-starbursts consists mostly of galaxies which have similar early-type structural properties to red sequence galaxies of comparable masses (Wong et al. 2012).

Earlier attempts to map the HI content of post-starburst galaxies only found HI in one of five targets which

consisted of an interacting pair of galaxies (Chang et al. 2001). All subsequent campaigns to detect HI in post-starbursts have been optimised towards detecting diffused low-surface brightness gas, while compromising on the angular resolution required to map the location of the gas (e.g. Zwaan et al. 2013).

To determine the physical process responsible for shutting down star formation, we posit that post-starburst galaxies are too evolved and that *the smoking gun for quenching is more likely to be found in its predecessor population, namely, the blue early-type galaxies.*

Using the Westerbork Syntheses Radio Telescope, we study the HI content of a pilot sample of four blue early-type galaxies—the progenitors to post-starburst galaxies because 1) these galaxies are still currently star-forming and therefore there should be gas where there are stars being formed; and 2) the state of the gas morphology and dynamics will shed light on why these galaxies will soon stop forming stars.

Section 2 describes the blue early-type sample. The pilot observations and data processing methods are described in Section 3. We discuss the radio continuum and HI imaging results in Section 4 and Section 5, respectively. Section 6 provides a summary of our results. The AB magnitude system is used throughout this work.

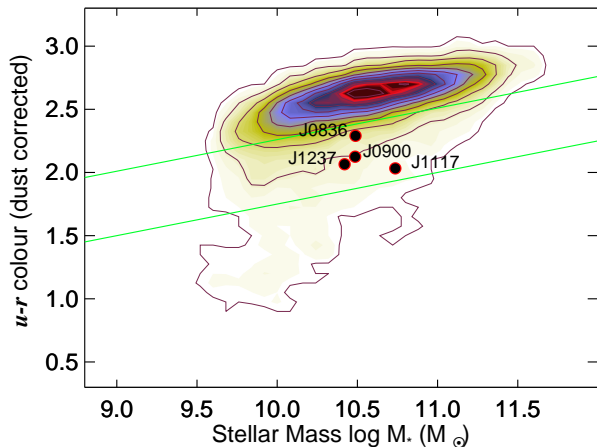


Figure 2. Colour-stellar mass diagram of ETGs found from SDSS and Galaxy Zoo. The contours represent the number density of ETGs occupying the colour-stellar mass region known as the ‘red sequence’. All four pilot sample galaxies are located in the optical ‘green valley’ of the colour-mass diagram (as demarcated between the solid green lines). All galaxies show the presence of intermediate age stellar populations by their ‘green’ $u - r$ colour.

2 BLUE EARLY-TYPE GALAXIES

We obtain the photometric and spectroscopic data from the Sloan Digital Sky Survey (SDSS) DR7 (York et al. 2000; Abazajian et al. 2009) for all objects classified as ‘galaxy’ (Strauss et al. 2002). The sample of 204 low-redshift ($0.02 < z < 0.05$) blue ETGs were identified using the Sloan Digital Sky Survey (Adelman-McCarthy et al. 2008, SDSS;) and the Galaxy Zoo project (Lintott et al. 2008; Schawinski et al. 2009; Lintott et al. 2011). The blue ETGs account for 5.7% of all ETGs found within the same redshift range and are the most actively star-forming population of ETGs (Schawinski et al. 2009). Further description of the blue early-type galaxy selection can be found in Schawinski et al. (2009) and at <http://data.galaxyzoo.org>.

2.1 The pilot sample

To investigate the fate of the gas reservoir when star formation is quenched, we select four ETGs with comparable stellar masses and UV/optical colours indicative of rapid quenching: all four lie in the optical $u - r$ green valley, indicating they have significant intermediate-age stellar populations, and their $NUV - u$ UV/optical colours range from very blue, consistent with ongoing star formation (J1237+39), to the redder colours of passive, quenched galaxies (J0836+30)—see Figure 2. Due to the diffused nature of HI gas, we have also selected the nearest galaxies which can be observed by the Westerbork Synthesis Radio Telescope (WSRT). The optical/stellar morphologies of this sample are presented in the top row of Figure 1.

Stellar population modelling find two distinct star formation truncation timescales for early- and late-type galaxies whereby the early-type galaxies appear to have fast quenching timescales (≤ 1 Gyr), while the late-type galaxies

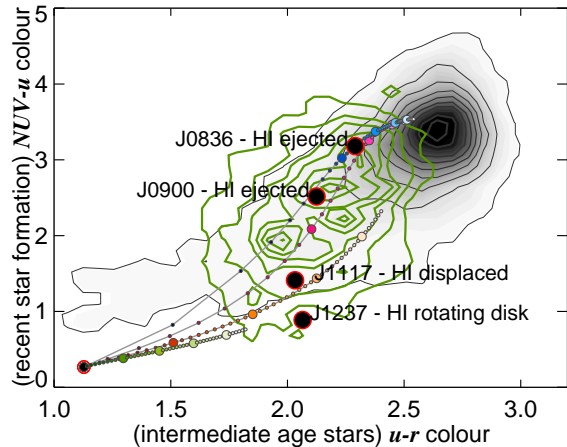


Figure 3. The UV/optical colour-colour diagrams of blue early-type galaxies (green density contours) and the entire early-type galaxy population (black shaded contours). The model stellar population tracks with varying quenching timescales from Schawinski et al. (2014) are also overlaid. The large and small circles along the evolutionary tracks represent 1 Gyr and 100 Myr, respectively. Two out of four pilot sample galaxies show an absence of very young stellar populations indicated by red $NUV - u$ colours. Those three galaxies also show either a displaced HI reservoir (J1117+51) or a completely ejected HI reservoir (J0836+30 and J0900+46). The galaxy which is bluest in $NUV - u$ features a rotating HI disk.

have quenching timescales of several Gyrs (Schawinski et al. 2014). Figure 3 illustrates the different evolutionary stages represented by each of the four ETGs selected for this pilot study on a UV/optical colour-colour diagram. The colour of model stellar populations along different star formation quenching tracks are shown as solid lines where each large circle marks 1 Gyr and intervals of 100 Myr being shown by small circles along the stellar evolution tracks. The black shaded contours represent the low-redshift early-type population and the green contour represents the population of blue early-type galaxies selected from Schawinski et al. (2009). The observed stellar populations of J0836+30 and J0900+46 appear to be relatively evolved along the fastest quenching evolutionary pathway that occurs on timescales of several hundred Myr to 1 Gyr (Schawinski et al. 2014). On the other hand, the stellar population colours of J1117+51 and J1237+39 are less evolved and consistent with earlier stages of quenching. We note that J1117+51 and J1237+39 appear to favour slower quenching pathways in Figure 3. However, this could be due to differences between the start times for quenching in these galaxies relative to the fiducial starting point for quenching in the models. The HI properties of each sampled galaxy appears to be consistent with its respective evolutionary stage. See Section 5 for more details of the observed HI properties of this sample.

In addition, all four galaxies show optical emission lines dominated by activity other than star formation: J0836 and J0900 show Seyfert-like lines while J1117 and J1237 show low-ionization lines which could be due to black hole accretion, shocks or evolved stars (Sarzi et al. 2010). Figure 4 presents the Baldwin, Phillips & Tevich (BPT) diagnostic

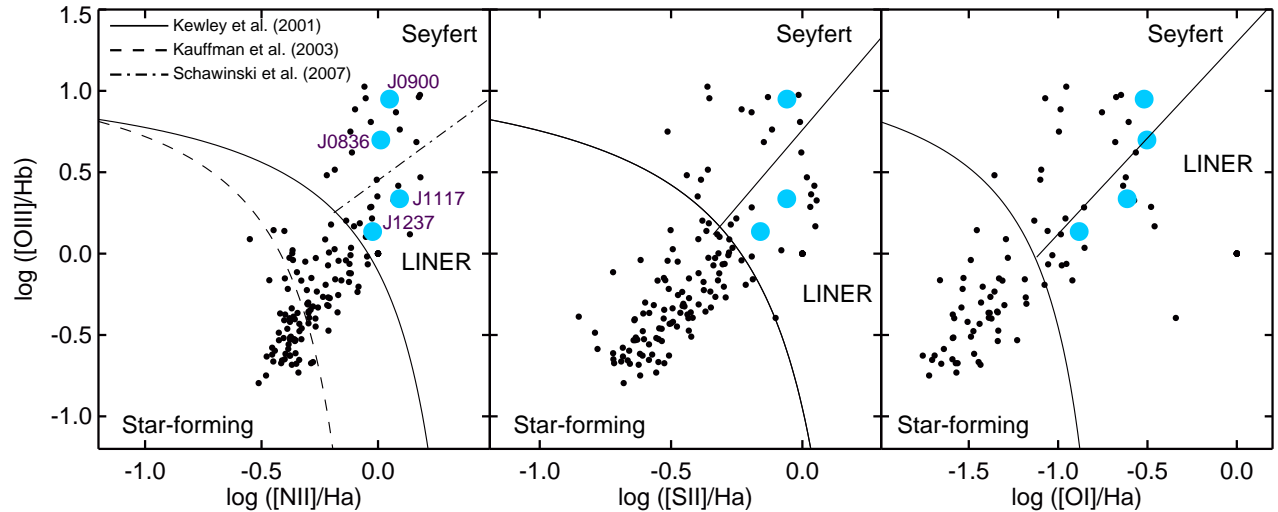


Figure 4. Optical nebular emission line diagrams. The nebular emission line ratios of the entire Schawinski et al. (2009) sample of blue early-type galaxies are plotted as black points. The blue solid points represent the objects selected in this pilot sample. The solid and dashed line are two lines used to separate the nebular emission originating from star formation rather than that of Seyfert or LINER activity (Kewley et al. 2001; Kauffmann et al. 2003). The dotted-dashed line differentiates between ionisation levels obtained from LINER versus Seyfert cores (Schawinski et al. 2007).

diagram (Baldwin et al. 1981) which shows the emission line ratios observed for blue early-type galaxies. Table 1 lists the optical properties of this pilot sample. Stellar masses were obtained from spectral fitting (Schawinski et al. 2009).

3 PILOT SURVEY

3.1 Radio observations

We performed imaging of the 1.4 GHz radio continuum and the atomic Hydrogen (HI) emission of our pilot sample using the WSRT in the Netherlands between June and November 2012. As the WSRT is an east-west interferometer, our observations were divided into several epochs to optimise the uv -coverage. The single 20 MHz band is sampled over 1024 channels in the maxi-short baseline configuration in order to obtain a spectral resolution of 4 km s^{-1} spanning the range of 4000 km s^{-1} .

Using this setup, a 24-hour on-source integration should result in an RMS noise level of $0.54 \text{ mJy beam}^{-1}$ at full angular resolution over a FWHM of 8.25 km s^{-1} in velocity—corresponding to a column density sensitivity of $1.46 \times 10^{19} \text{ atoms cm}^{-2}$ per resolution assuming a uniform weighting¹. Due to timetabling constraints, we were not able to obtain 24-hour on-source integration for each of the four galaxies. Total integration times for each galaxy, the resultant synthesised beam properties and sensitivities are listed in Table 2.

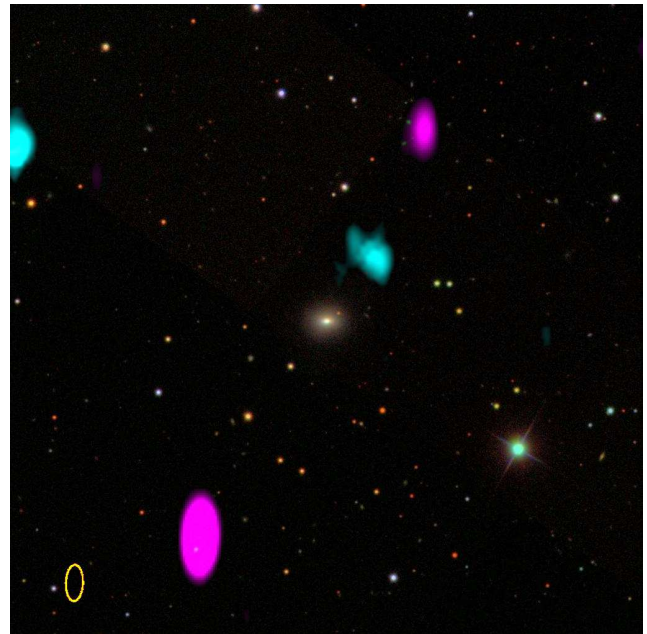


Figure 5. Multicolour composite of the J0836+30 field (centred on J0836+30) where the background colour image is a multicolour composite of the five SDSS optical $ugriz$ bands. The 1.4 GHz radio continuum and HI emission from these pilot observations are shown in magenta and cyan, respectively. The yellow ring in the bottom-left of the figure represents the beam of the radio observations.

3.2 Data processing

The observations are calibrated and processed in the standard manner using the MIRIAD Reduction software

¹ Noise estimations are obtained from the WSRT exposure time calculator found at <http://www.astron.nl/oosterlo/expCalc.html>

Table 1. Optical properties of our low-redshift blue early-type galaxy sample.

SDSS ID (1)	Galaxy (2)	RA (J2000) (3)	Declination (J2000) (4)	Redshift (5)	Distance (6)	r (7)	$u - r$ (8)	$\log(M_*)$ (9)
587735044686348347	J0836+30	08:36:01.5	+30:15:59.1	0.02561	105	-21.1	2.27	10.7
587731887888990283	J0900+46	09:00:36.1	+46:41:11.4	0.02748	113	-21.3	2.20	10.5
587732135382089788	J1117+51	11:17:33.3	+51:16:17.7	0.02767	115	-21.4	2.33	10.6
587738946685304841	J1237+39	12:37:15.7	+39:28:59.3	0.02035	84	-20.9	2.16	10.3

Col. (1): SDSS object identification. Col. (2): Galaxy identification used in this paper. Col. (3): Galaxy center's right ascension. Col. (4): Galaxy center's declination. Col. (5): Redshift. Col. (6): Distance in Mpc. Col. (7): SDSS r -band magnitude. Col. (8): Optical $u - r$ colour. Col. (9): \log (stellar mass) in solar mass as estimated by spectral fitting.

Table 2. WSRT observation summary. WSRT observation integration times and resulting beam properties are detailed for each of our pilot blue galaxies.

Galaxy (1)	Observations dates (2)	Total integration time (3)	Beamsize (4)	Beam Position angle (5)	RMS_{HI} (6)	$\text{RMS}_{1.4}$ (7)
J0836+30	Nov 15,25	20.3	29.5, 13.9	-2.0	4.1	0.083
J0900+46	Oct 23, Nov 11	10.3	24.0, 12.1	-1.7	11.0	0.062
J1117+51	June 30, Nov 18	24.0	19.8, 14.5	9.6	3.7	0.082
J1237+39	Aug 24, Oct 25, Nov 21	24.2	27.6, 17.5	4.7	32.6	0.038

Col. (1): Galaxy identification. Col. (2): Observation dates. Col. (3): Total on-source integration time in hours. Col. (4): Synthesised beam diameter in arcseconds. Col. (5): Synthesised beam position angle in degrees. Col. (6): RMS noise level for the HI emission in mJy beam⁻¹. Col. (7): RMS noise level for the 1.4 GHz radio continuum in mJy beam⁻¹.

(Sault et al. 1995). After the initial bandpass calibration using a WSRT standard calibrator, continuum images are produced and improved by iteratively applying a continuum self-calibration. The resulting calibration tables are then used for the line imaging as well. After a second continuum subtraction, the resulting HI image cubes are produced by using a robust weighting of 0.4 in order to produce the optimal balance between angular resolution and surface brightness sensitivity. We average across every second channel to improve the signal-to-noise sensitivity which results in a velocity resolution of 8.5 kms⁻¹ (after Hanning smoothing). It should be noted that these final reduction parameters were determined after we had already tested various combinations of weighting schemes (including natural and uniform weightings) with different angular and frequency tapering for each set of observations. Table 2 lists the RMS levels obtained for each galaxy in our sample.

4 RADIO CONTINUUM PROPERTIES OF BLUE EARLY-TYPE GALAXIES

We observe 1.4 GHz radio continuum emission in the nuclear regions of J0900+46, J1117+51 and J1237+39. No nuclear radio emission was found for J0836+30, but we do observe two radio lobes extending 88.4 kpc north-west and 102.5 kpc south-east of J0836+30 along the same direction as the extragalactic HI cloud. Figure 5 shows a multicolour composite image of the J0836+30 field where the radio continuum and the integrated HI emission is shown in magenta and cyan, while the background three-colour image is produced from the five SDSS *ugriz* bands. Further discussion of the pos-

sible mechanism for the displacement of the HI reservoir in J0836+30 can be found in Section 5.1.

We argue that the two radio lobes flanking both sides of J0836+30 are likely to be faded radio lobes belonging to J0836+30 and not likely to be due to a chance alignment with background sources. Although there is some overlap between the South-Eastern radio lobe with a WISE 3.6 micron source, we do not find an optical/IR counterpart for the North-Western radio lobe. In addition, the projected separation between both lobes and J0836+30 are similar enough for the differences in angular separation (as well as brightness) to be accounted for by projection effects.

The nuclear radio luminosities range from 2.0×10^{35} to 7.4×10^{35} ergs s⁻¹ (or 1.0×10^{20} to 3.7×10^{21} W Hz⁻¹) and are consistent with those found mostly in other radio studies of low-redshift star-forming galaxies (Mauch & Sadler 2007; Jarvis et al. 2010). For J0836+30, the luminosities of the radio lobes in the north-west and south-east directions are 9.26×10^{35} and 1.22×10^{37} ergs s⁻¹, respectively. Table 3 lists the measured 1.4 GHz radio continuum properties. Figure 1 shows the radio continuum emission as green contours and the HI emission as white contours for the entire pilot sample.

Assuming that the nuclear radio continuum emission is due to star formation, we can estimate the star formation rate upper limits in our pilot sample. Using the star formation rate calibrations from Bell (2003); Hopkins et al. (2003), we find that our galaxies have star formation rates that are fewer than 2 solar mass per year. J1117+51 has the highest estimated star formation rate with 1.7 solar mass per year.

Archival IRAS 60 μm observations (Moshir & et al. 1990) were found for J1117+51 and J1237+39. Using the far-infrared to radio correlation (FRC) of low-redshift star-

forming galaxies Yun et al. (2001), we find that the expected far-infrared $60\ \mu\text{m}$ luminosity that correlates to our measured radio luminosity if the radio emission is due solely to star formation is $\log L_{60}$ of 9.6 and 9.0 for J1117+51 and J1237+39, respectively. In comparison to the IRAS $\log L_{60}$ values of 9.4 and 9.3, we find that the predicted values from the FRC are consistent with the idea that the 1.4 GHz continuum emission originates from star formation for both J1117+51 and J1237+39. It should be noted that the FRC has a scatter of approximately 0.25 dex and the IRAS measurement uncertainties are at the 20% level.

Although the radio continuum emission observed from J1237+39 appears to be extended, it is in fact the result of a chance alignment between J1237+39 and a projected background galaxy, SDSS J123716.92+392921.9, which is 8.5 times more distant (at redshift $z = 0.176$) than J1237+39. Figure 6 shows that the observed radio emission can be simply modelled by two point sources. The lack of any regions which display a flux excess or a flux deficit in our residual image (panel c of Figure 6) is consistent with the idea that the radio emission from J1237+39 does not have an extended diffuse component.

5 HI CONTENT OF BLUE EARLY-TYPE GALAXIES

As the four blue ETGs in our sample represent four separate stages of evolution (as traced by the UV/optical colours and the $[\text{OIII}]/[\text{H}\beta]$ ratios), we observe a correlation with their respective HI gas-to-stellar mass fractions whereby the gas fractions decrease as a function of time with increasing UV/optical colours and increasing $[\text{OIII}]/[\text{H}\beta]$ ratios. Table 3 lists the measured HI properties. The galaxy at the earliest stage of quenching in our sample (i.e. the galaxy with the bluest NUV/optical colour and the weakest $[\text{OIII}]/[\text{H}\beta]$ ratio), J1237+39, features a central, undisturbed, rotating HI disk. Both spatial and kinematic asymmetries are not observed in this galaxy (see Figure 1 and Figure 7).

In the second bluest galaxy, J1117+51, the HI gas appears to be mostly within J1117+51. However the gas morphology is fairly asymmetric and appears offset from the optical centre of the galaxy. Assuming the optical velocity to be the systemic velocity of each galaxy, we find the HI gas in J1117+51 to be largely blue-shifted by up to $170\ \text{kms}^{-1}$ from the galaxy's systemic velocity (see Figure 7).

In the redder galaxies and the galaxies with stronger $[\text{OIII}]/[\text{H}\beta]$ ratios—indicative of ionisation levels consistent with Seyfert activity, the HI reservoirs of J0836+30 and J0900+46 are completely displaced from their respective galaxy centres by 14–86 kiloparsecs. In addition, we find a significant amount of red-shifted HI (by $\approx 70 - 80\ \text{kms}^{-1}$) with respect to the systemic velocity of the individual galaxy (see Figure 1).

In J0836+30, the entire gas reservoir is offset spatially by 1 arcminute (projected distance of 30.5 kpc). To approximate the timescale for the displacement of the gas reservoirs from J0836+30 and J0900+36, we simply divided the projected distances of the gas clouds by the observed HI velocity offsets from the systemic velocities taken from the optical observations. For J0836+30, the timescale for the gas reservoir to have reached its current projected distance

is approximately 373 Myr. Similarly, the HI emission detected near J0900+46 spans between 14 kpc to 86 kpc from the optical center of J0900+46 and appears to be redshifted by approximately $70\ \text{kms}^{-1}$ (Figure 8b). We estimate the displacement timescale to range between 0.2 to 1.2 Gyr.

5.1 Mechanisms for the removal of HI

Support for the hypothesis that the observed HI clouds in the vicinity of J0836+30 and J0900+46 have been removed from their parent galaxy come from two main arguments. Firstly, the proximity of the gas clouds are very similar to the distances between the Milky Way and its high velocity clouds (HVCs). Secondly, neither J0836+30 nor J0900+46 reside in dense environments with close neighbouring galaxies which could be responsible for stripping the gas reservoirs from each of these galaxies. In fact, Verley et al. (2007) has that found both J0836+30 and J0900+46 to be isolated galaxies using different galaxy isolation metrics. Several other previous studies have also classified J0836+30 to be a prototypical isolated galaxy (Verdes-Montenegro et al. 2005; Stocke et al. 2004; Karachentseva 1973).

In dense galaxy environments, such as clusters or compact galaxy groups, intergalactic gas clouds are not uncommon (Kilborn et al. 2000; Oosterloo & van Gorkom 2005; Borthakur et al. 2010) due to various gravitational and hydrodynamic interaction processes such as galaxy-galaxy interactions (Mihos 2004), harassment (Moore et al. 1996, 1998), ram pressure and turbulent viscous stripping (Vollmer et al. 2001).

Ram pressure stripping is unable to shift such large amounts of gas using simple Toomre & Toomre pressure arguments (e.g. Chung et al. 2007). Also, the galaxies in this pilot sample do not have nearby galaxy neighbours nor do they reside in dense galaxy environment such as clusters or compact groups.

Nearby examples where the majority of the galaxy's gas is displaced via tidal stripping also results in strong morphological distortions (e.g. NGC 4438 in the Virgo Cluster (Hota et al. 2007)). Hota et al. (2012) has also identified a post-merger system, NGC 3801, where the extraplanar HI resulting from the merger has yet to be encountered by a newly-triggered radio jet. As we do not observe any strong optical signatures from our galaxies such as stellar tidal tails, we can only infer that (1) the tidal features resulting from the strong interaction that removed the large gas mass have faded; or (2) another physical mechanism is responsible for the gas removal.

In the latter case, we posit that an active central engine has the required energy to expel a galaxy's gas. In the case of J0836+30, we observe two radio lobes in the same direction as the ejected HI cloud. This is suggestive that at earlier epochs, J0836+30 hosted a radio AGN which may have blown out the gas cloud that we observe. This hypothesis is consistent with recent studies which have found nuclear activity to be more prevalent in star-forming galaxies relative to weakly star-forming or quenched galaxies (Rosario et al. 2013).

As the displacement timescale for this cloud is estimated to be ≈ 373 Myr, it is conceivable that J0836+30 has since evolved to a more Seyfert state (as observed via the optical nebular emission). A test of this hypothesis would

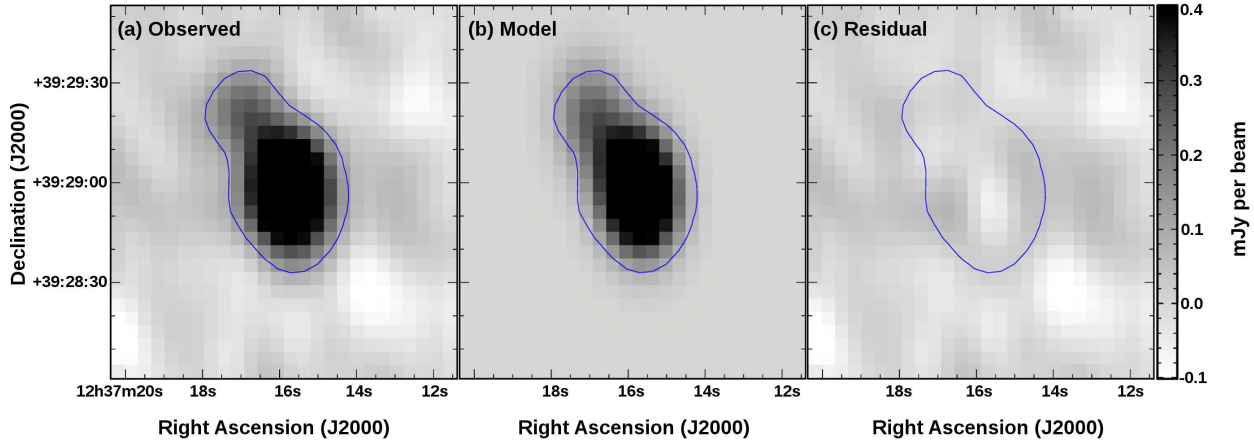


Figure 6. The 1.4 GHz radio continuum emission from J1237+39. Centred on J1237+39, we model the emission as two overlapping point sources. The solid blue line in all three panels mark the 3σ flux level of the observed 1.4 GHz emission (see Panel a). Panels b and c show the model of two point sources and the residual maps, respectively.

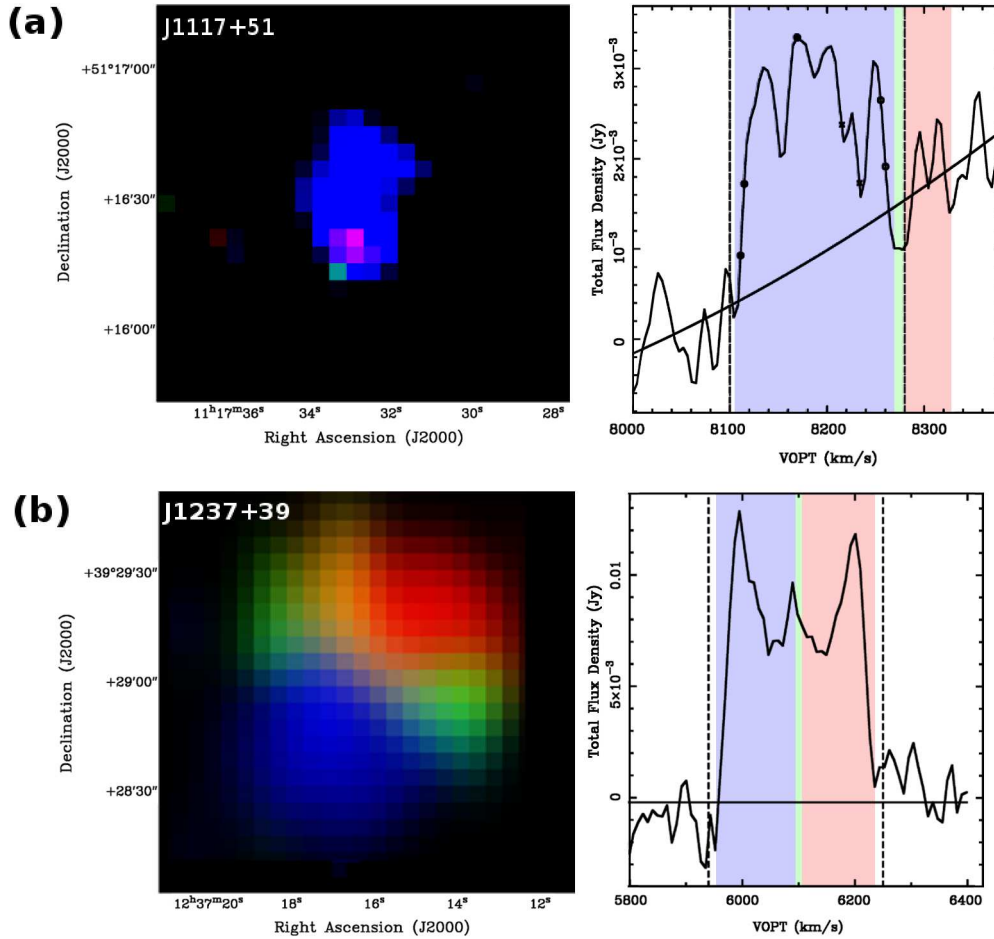


Figure 7. Velocity maps and spectra of J1117+51 (panel a) and J1237+39 (panel b). The 3-color velocity maps correspond to the HI emission in the velocity range highlighted in the same color on the corresponding velocity spectrum. It should be noted that the green represents the optical velocity which we assume to be the systemic velocity of each of the blue early-types sampled in this paper.

Table 3. Radio (1.4 GHz) and HI properties of blue early-type galaxies.

Galaxy (1)	$S_{1.4}$ (2)	$L_{1.4}$ (3)	$L_{1.4}$ (4)	$SFR_{1.4}$ (5)	S_{HI} (6)	v_{HI} (7)	w_{HI} (8)	M_{HI} (9)
J0836+30	$< 2.5 \times 10^{-4}$	$< 3.3 \times 10^{20}$ **	$< 6.6 \times 10^{34}$	< 0.4	0.078 (0.025)	7705	140	2.0 (0.7)
J0900+46	$9.7(2.4) \times 10^{-4}$	1.5×10^{21}	3.0×10^{35}	1.1	0.410 (0.182)	8277	62	12.3 (5.5)
J1117+51	$23.4(3.8) \times 10^{-4}$	3.7×10^{21}	7.4×10^{35}	1.7	0.100 (0.020)	8185	140	3.1 (0.6)
J1237+39	$12.0(1.6) \times 10^{-4}$	1.0×10^{21}	2.0×10^{35}	0.7	2.448 (0.403)	6096	245	40.8 (6.7)

**Note that the luminosities of the radio lobes in the north-west and south-east directions are $4.63 (\pm 0.44) \times 10^{21} \text{ WHz}^{-1}$ and $6.12 (\pm 0.03) \times 10^{22} \text{ WHz}^{-1}$, respectively. Col. (1): Galaxy identification. Col. (2): Total 1.4 GHz radio continuum emission in Jansky. Col. (3): Radio continuum luminosity (1.4 GHz) in WHz^{-1} . Col. (4): Radio continuum luminosity (1.4 GHz) in ergs s^{-1} . Col. (4): Estimated star formation rate using the calibration by Bell (2003); Hopkins et al. (2003) in $M_{\odot} \text{ year}^{-1}$. Col. (5): Integrated HI emission in Jansky. Col. (6): HI radial velocity as measured from the mid-point at full-width half-maximum in kms^{-1} . Col. (7): The 50% HI velocity width in kms^{-1} . Col. (8): Total HI mass in units of $\times 10^8 M_{\odot}$. Values in brackets give the estimated errors.

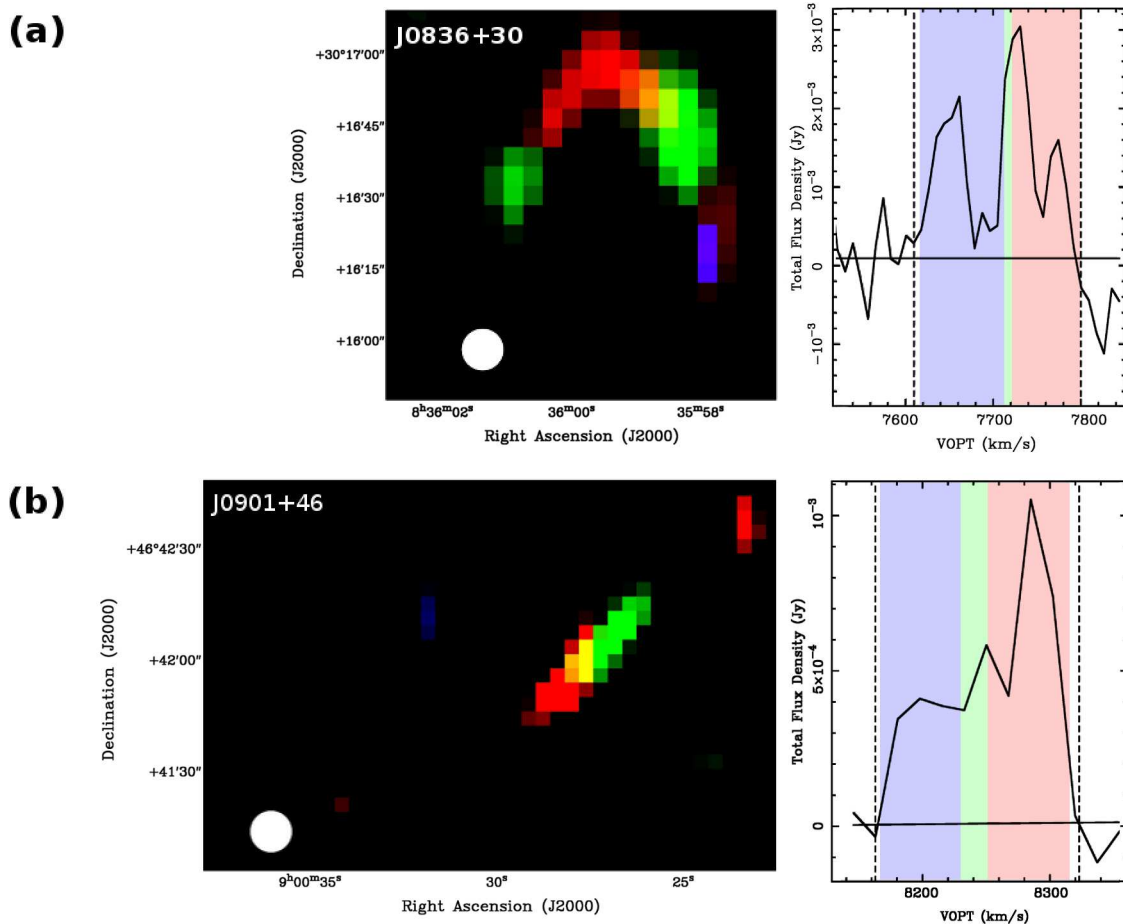


Figure 8. Velocity maps and spectra of J0836+30 (panel a) and J0900+46 (panel b). The 3-color velocity maps correspond to the HI emission in the velocity range highlighted in the same color on the corresponding velocity spectrum. The white solid circle represents the position of the blue early-type galaxy relative to the observed HI emission. It should be noted that the green represents the optical velocity which we assume to be the systemic velocity of each of the blue early-types sampled in this paper.

be the presence of ionized gas adjacent to and between the observed HI cloud and the galaxy. Therefore, in the case of J0836+30, we think that the alignment between the radio lobes and the extragalactic HI cloud is more suggestive of gas ejection via radio jets than a previous tidal encounter whose tidal signatures have since faded in the past 373 Myr. Previous observations of AGN-driven gas outflows have

so far been from studies where the outflows are determined from the kinematic structures of the emitting or absorbing gas (Gopal-Krishna & Irwin 2000; Nesvadba et al. 2009; Mahony et al. 2013; Morganti et al. 2013). However, recent observations of $^{12}\text{CO}(1-0)$ emission from high-redshift radio galaxies have found spatial offsets between the molecular gas reservoir and their host galaxies on the scales of several

tens of kiloparsecs and aligned in the same direction to the radio hotspots/lobes (Emonts et al. 2014). We propose that we are witnessing a similar ejection of cold gas in J0836+30.

In the case of J0900+46, we neither observe strong radio continuum emission nor nearby galaxies which could remove the gas from this galaxy.

We posit that the observed extragalactic gas clouds in J0836+30 and J0900+46 are outflows and not inflows for two reasons. Firstly, if the observed cold clouds were being accreted, the source of this gas is either a neighbouring galaxy or primordial gas leftover from galaxy formation. However, neither galaxies have neighbouring galaxies and the accretion of primordial gas at the current epoch is in a warm-hot phase rather than that of the observed cold HI. Secondly, Bouché et al. (2012) found that gas outflows are usually found at angles nearly orthogonal (> 60 degrees) to the plane of the galaxy, whereas inflows have small azimuthal angles (< 30 degrees) the galactic plane. Therefore, we think that it's more likely that our observed extragalactic HI clouds originated from our target galaxies.

The mass of our gas clumps are approximately the total mass of HVCs around the Milky Way, the LMC and the SMC. Assuming that our observed gas clumps are analogous to these HVCs, we can expect a similar gas dissipation time on the order of several hundred million years if there isn't some sort of support mechanism that prevents or slow down against cloud dissipation (Putman et al. 2012). The cloud survival time is linked closely to its total mass, cloud density, relative halo density and velocity (Putman et al. 2012). Previous studies have found that while the least bound material is likely to expand out into the IGM, bound structures are likely to fall back onto the galaxies in less than 1 Gyr (Hibbard & Mihos 1995; Hibbard & van Gorkom 1996).

5.2 HI gas fractions

Using the scaling relations from the $\alpha 40$ catalog of the ALFALFA survey (Huang et al. 2012), star-forming galaxies with the stellar masses of J0836+30 and J0900+46 would be expected to have average HI masses of approximately $1 \times 10^{10} M_{\odot}$ and $8.7 \times 10^9 M_{\odot}$, yet we observe only $2 \times 10^8 M_{\odot}$ and $1.2 \times 10^9 M_{\odot}$, respectively. This implies that some fraction of the gas may have been ionized and heated and we are currently only observing the remaining fraction of HI. The external HI clouds we observe represent the remnants of the original gas reservoirs swept out of the host galaxy, and from the present data it is not clear whether the missing HI was also expelled or heated or simply dissipated. Regardless, the displaced gas reservoir is required to complete the quenching of these galaxies and prevent further star formation.

Extrapolating from the Kennicutt-Schmidt star formation law, the correlation between the HI gas fraction and the star formation history traced by the NUV- r color provides a rough indicator for the cold gas surface density (Huang et al. 2012; Zwaan et al. 2013). Relative to gas-rich star-forming galaxies (mostly spirals) (ALFALFA; Huang et al. 2012), low-redshift transition galaxies with stellar masses greater than $10^{10} M_{\odot}$ (GASS; Catinella et al. 2012) and nearby early-type galaxies from the Atlas3D survey (Serra et al. 2012; Cappellari et al. 2013; Young et al. 2013), we find that J1117-51 and J1237+36 have similar gas fractions and

NUV- r colors to E+A galaxies and straddle the region between star-forming galaxies with low gas fractions and that of gas-rich early-type galaxies.

Figure 9 compares the HI-stellar mass ratio and the integrated NUV- r colour of J1117+51 and J1237+39 (marked as black stars) to those of E+A galaxies (represented by black crosses) where HI has been previously detected (Chang et al. 2001; Buyle et al. 2006; Helmboldt 2007; Zwaan et al. 2013).galaxies from ALFALFA are represented by blue solid points and the solid line marks the average colours and average gas fractions found from GASS. Near-ultraviolet (NUV) measurements of our sample were obtained from the Galex satellite telescope via the NASA Extragalactic Database².

We also compare our pilot sample of blue ETGs to recent HI observations of nearby ETGs from the Atlas3D survey (Serra et al. 2012). The Atlas3D ETGs with regularly-rotating undisturbed HI morphologies are represented by open circles, while, Atlas3D galaxies with very disturbed and unsettled HI morphologies and kinematics are represented by solid diamonds in Figure 9. It should be noted that all the Atlas3D ETGs with disturbed HI morphologies reside in group or Virgo Cluster environments. Also, for a given NUV- r colour, these Atlas3D galaxies have higher gas fractions than that of the E+A or blue ETG samples. This suggests that either (1) the Atlas3D ETGs where HI is observed are at earlier stages of evolution than the sample of E+A galaxies or blue ETGs; or that (2) the merger scenario is as likely to result in an increase in gas fraction as it is to a reduction. Upper limits are shown for J0836+30 and J0900+46 due to the lack of HI within the host galaxies.

We find the HI gas fraction and NUV- r colour of J1237+39 (the galaxy at the earliest stage of quenching) to be very comparable to those of star-forming galaxies from both the ALFALFA and GASS surveys. On the other hand, the gas fractions for the three more evolved blue ETGs in our sample are significantly lower than the average gas fractions expected from star-forming galaxies, transitioning galaxies or even gas-rich early-type galaxies with similar NUV- r colours. Similar to our results, the gas fractions of post-starburst E+A galaxies are lower than the average gas fractions for any given NUV- r colours. The combination of the HI mapping and the radio continuum observations of J0836+30 and J0900+46 suggest that the star formation in these two galaxies will be truncated soon. This result is consistent with those of Schawinski et al. (2009) who were unable to detect any significant molecular gas reservoirs within Green Valley galaxies with Seyfert ionisation properties.

As previously seen in Figure 3, these pilot HI observations show that the main mechanism for the fast quenching of star formation in blue early-types is due to the physical displacement of the main gas reservoir from which stars are formed. Hence, it is likely that the depressed gas fractions from our sample (see Figure 9) are due to a fast quenching process (relative to other evolving galaxies) which removes a significant fraction, if not the entire gas reservoir, from which stars are formed.

Should the gas fall back, it may restart minor star formation which may be visible as the frosting $\approx 1\%$

² <http://ned.ipac.caltech.edu>

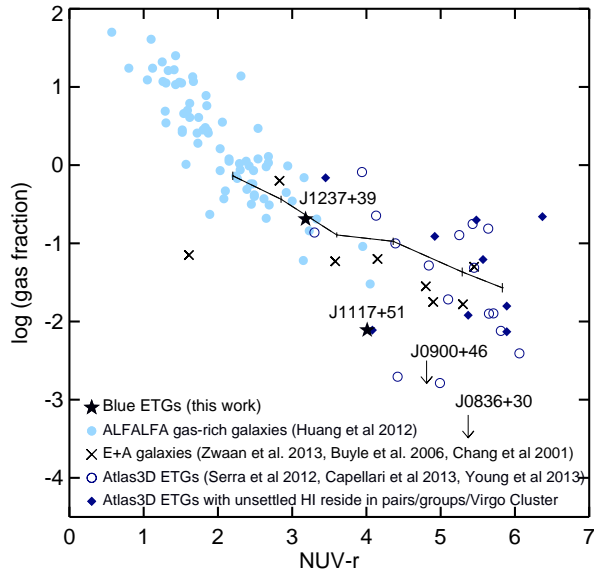


Figure 9. HI-to-stellar mass ratio as a function of galaxy color. The solid line shows the average gas fractions found from GASS survey of massive transition-type galaxies (Catinella et al. 2012).

mass fraction of young stars often observed in quenched early-type galaxies (Yi et al. 2005; Schawinski et al. 2006; Kaviraj et al. 2007). While it may cause frosting, this returning gas however will not return the host galaxy to self-regulated star-formation on the main sequence. An alternative fate for the ejected gas is that it persists at large distances from the quenched galaxy, as is observed in the Milky Way (in the form of the starless Magellanic stream; For et al. 2014); as well as in many quenched early-type galaxies (e.g. Serra et al. 2012).

5.3 Argument against coincident dark galaxies

Dark galaxies can be typically defined as the extreme end of low surface brightness galaxies where few stars are found, consisting mainly of gas. With respect to our observed extraplanar gas clumps, it is very unlikely that these gas clumps are neighbouring dark galaxies. Current re-ionization models of the Universe predict the latter as they find that the gas from 95 per cent of the low-mass systems ($M_{\text{virial}} \leq 10^8 M_{\odot}$ or $v_{\text{circ}} \leq 20 \text{ km s}^{-1}$) appears to have been photoevaporated during the epoch of re-ionization (Susa & Umemura 2004).

Apart from a few reported cases of extragalactic gas clouds in group/cluster environments (Minchin et al. 2005; Davies et al. 2006)) with no known optical counterparts, current and previous HI all-sky surveys such as ALFALFA (Haynes et al. 2011) and HIPASS (Wong et al. 2009; Doyle et al. 2005) have not found any isolated extragalactic HI clouds devoid of stars. This is consistent with simple gas equilibrium models (Taylor & Webster 2005) which concluded that in the absence of an internal radiation field, dark galaxies/gas clouds with masses greater than $10^9 M_{\odot}$ will become Toomre unstable against star formation and start forming stars. Galaxy evolution simulations demonstrated

that the majority of gas clouds identified with no known optical counterpart can be easily reproduced by galaxy–galaxy interactions (Bekki et al. 2005; Duc & Bournaud 2008).

6 SUMMARY

We have performed deep imaging of the HI content and 1.4 GHz radio continuum emission of four blue early-type galaxies that are at four different stages of star formation truncation using the WSRT. The HI morphologies, kinematics and relative HI-gas fractions are excellent probes and measures of the quenching evolutionary stages for each of our sample galaxy. A summary of our results are as follows:

(i) We observe nuclear 1.4 GHz radio continuum emission that are consistent with emission from star formation from three galaxies at the three earliest stages of quenching evolution, namely, J1237+39, J1117+51 and J0900+46 (in the order of earliest to later stages of evolution).

(ii) The galaxy at the earliest stage of quenching, J1237+39, also has the bluest $\text{NUV}-r$ colour, weakest $[\text{OIII}/\text{H}\beta]$ ratio, the highest HI gas fraction and a symmetric rotating HI disk.

(iii) At more advanced stages of quenching evolution, we observe increasingly asymmetric and increased spatial offsets between the HI gas and the stellar component of the galaxy. Non-rotating HI gas kinematics are also observed. In the case of the two galaxies at the most advanced stages of evolution where Seyfert ionisation signatures have been observed (J0900+46 and J0836+30), the HI gas reservoirs have been entirely expelled by approximately 14–86 kpc from their respective host galaxies. Due to the lack of neighbouring galaxies, it is difficult to attribute the stripped gas to tidal or ram pressure interactions.

(iv) In the galaxy at the most advanced quenching stage, J0836+30, the expelled gas reservoir is observed to be in alignment between the host galaxy and two radio lobes—suggesting the gas reservoir may have been swept out of the galaxy by powerful outflows from the central AGN in a previous active phase. This scenario is consistent with recent observations of AGN-driven gas outflows both locally and at higher redshifts (Sturm et al. 2011; Mahony et al. 2013; Morganti et al. 2013; Emonts et al. 2014).

(v) We conclude that the rapid quenching of star formation in low-redshift early-type galaxies is due to the physical expulsion of the entire gas reservoir, rather than the exhaustion of gas via star formation. An AGN outflow has the necessary energy to expel the reservoir of cold gas. In addition, we do not think that AGN heating of the gas is a dominant mechanism because the HI gas would not remain visible as a coherent structure if this was the case.

Acknowledgments. We thank the anonymous referee for their support of this project and for improving the manuscript. OIW acknowledges a Super Science Fellowship from the Australian Research Council and the Helena Kluyver visitor programme at ASTRON/JIVE. KS is supported by SNF Grant PP00P2 138979/1. The Westerbork Synthesis Radio Telescope is operated by the ASTRON

(Netherlands Institute for Radio Astronomy) with support from the Netherlands Foundation for Scientific Research (NWO). This publication makes use of SDSS DR10 data. This research has made use of the NASA/IPAC Extragalactic Database (NED) which is operated by the Jet Propulsion Laboratory, California Institute of Technology, under contract with the National Aeronautics and Space Administration.

REFERENCES

- Abazajian K. N., Adelman-McCarthy J. K., Agüeros M. A., Allam S. S., Allende Prieto C., An D., Anderson K. S. J., Anderson S. F., Annis J., Bahcall N. A., et al. 2009, *ApJS*, 182, 543
- Adelman-McCarthy J. K., Agüeros M. A., Allam S. S., Allende Prieto C., Anderson K. S. J., Anderson S. F., Annis J., Bahcall N. A., et al. 2008, *ApJS*, 175, 297
- Ahn C. P., Alexandroff R., Allende Prieto C., Anders F., Anderson S. F., Anderton T., Andrews B. H., Aubourg É., et al. 2014, *ApJS*, 211, 17
- Alatalo K., Blitz L., Young L. M., Davis T. A., Bureau M., Lopez L. A., Cappellari M., Scott N., et al. 2011, *ApJ*, 735, 88
- Baldwin J. A., Phillips M. M., Terlevich R., 1981, *PASP*, 93, 5
- Bekki K., Koribalski B. S., Kilborn V. A., 2005, *MNRAS*, 363, L21
- Bell E. F., 2003, *ApJ*, 586, 794
- Borthakur S., Yun M. S., Verdes-Montenegro L., 2010, *ApJ*, 710, 385
- Bouché N., Dekel A., Genzel R., Genel S., Cresci G., Förster Schreiber N. M., Shapiro K. L., Davies R. I., et al. 2010, *ApJ*, 718, 1001
- Bouché N., Hohensee W., Vargas R., Kacprzak G. G., Martin C. L., Cooke J., Churchill C. W., 2012, *MNRAS*, 426, 801
- Buyle P., Michielsen D., De Rijcke S., Pisano D. J., Dejonghe H., Freeman K., 2006, *ApJ*, 649, 163
- Cappellari M., McDermid R. M., Alatalo K., Blitz L., Bois M., Bournaud F., Bureau M., Crocker A. F., et al. 2013, *MNRAS*, 432, 1862
- Catinella B., Schiminovich D., Kauffmann G., Fabello S., Hummels C., Lemonias J., Moran S. M., Wu R., et al. 2012, *A&A*, 544, A65
- Chang T.-C., van Gorkom J. H., Zabludoff A. I., Zaritsky D., Mihos J. C., 2001, *AJ*, 121, 1965
- Chung A., van Gorkom J. H., Kenney J. D. P., Vollmer B., 2007, *ApJ*, 659, L115
- Croston J. H., Hardcastle M. J., Kharb P., Kraft R. P., Hota A., 2008, *ApJ*, 688, 190
- Croton D. J., Springel V., White S. D. M., De Lucia G., Frenk C. S., Gao L., Jenkins A., Kauffmann G., et al. 2006, *MNRAS*, 365, 11
- Davies J. I., Disney M. J., Minchin R. F., Auld R., Smith R., 2006, *MNRAS*, 368, 1479
- Doyle M. T., Drinkwater M. J., Rohde D. J., Pimblet K. A., Read M., Meyer M. J., Zwaan M. A., Ryan-Weber E., et al. 2005, *MNRAS*, 361, 34
- Duc P.-A., Bournaud F., 2008, *ApJ*, 673, 787
- Elbaz D., Dickinson M., Hwang H. S., Díaz-Santos T., Magdis G., Magnelli B., Le Borgne D., Galliano F., et al. 2011, *A&A*, 533, A119
- Emonts B. H. C., Morganti R., Tadhunter C. N., Holt J., Oosterloo T. A., van der Hulst J. M., Wills K. A., 2006, *A&A*, 454, 125
- Emonts B. H. C., Norris R. P., Feain I., Mao M. Y., Ekers R. D., Miley G., Seymour N., Röttgering H. J. A., et al. 2014, *MNRAS*, 438, 2898
- For B.-Q., Staveley-Smith L., Matthews D., McClure-Griffiths N. M., 2014, *ApJ*, 792, 43
- Gopal-Krishna Irwin J. A., 2000, *A&A*, 361, 888
- Harrison C. M., Thomson A. P., Alexander D. M., Bauer F. E., Edge A. C., Hogan M. T., Mullaney J. R., Swinbank A. M., 2014, *ArXiv e-prints*
- Haynes M. P., Giovanelli R., Martin A. M., Hess K. M., Saintonge A., Adams E. A. K., Hallenbeck G., Hoffman G. L., et al. 2011, *AJ*, 142, 170
- Heckman T. M., Best P. N., 2014, *ARA&A*, 52, 589
- Helmboldt J. F., 2007, *MNRAS*, 379, 1227
- Hibbard J. E., Mihos J. C., 1995, *AJ*, 110, 140
- Hibbard J. E., van Gorkom J. H., 1996, *AJ*, 111, 655
- Hopkins A. M., Afonso J., Chan B., Cram L. E., Georgakakis A., Mobasher B., 2003, *AJ*, 125, 465
- Hota A., Rey S.-C., Kang Y., Kim S., Matsushita S., Chung J., 2012, *MNRAS*, 422, L38
- Hota A., Saikia D. J., Irwin J. A., 2007, *MNRAS*, 380, 1009
- Hota A., Sirothia S. K., Ohshima Y., Konar C., Kim S., Rey S.-C., Saikia D. J., Croston J. H., et al. 2011, *MNRAS*, 417, L36
- Huang S., Haynes M. P., Giovanelli R., Brinchmann J., 2012, *ApJ*, 756, 113
- Jarvis M. J., Smith D. J. B., Bonfield D. G., Hardcastle M. J., Falder J. T., Stevens J. A., Ivison R. J., Auld R., et al. 2010, *MNRAS*, 409, 92
- Karachentseva V. E., 1973, *Astrofizicheskie Issledovaniia Izvestiya Spetsial'noj Astrofizicheskoi Observatorii*, 8, 3
- Kauffmann G., Heckman T. M., Tremonti C., Brinchmann J., Charlot S., White S. D. M., Ridgway S. E., Brinkmann J., et al. 2003, *MNRAS*, 346, 1055
- Kaviraj S., Schawinski K., Devriendt J. E. G., Ferreras I., Khochfar S., Yoon S.-J., Yi S. K., Deharveng J.-M., et al. 2007, *ApJS*, 173, 619
- Kaviraj S., Schawinski K., Silk J., Shabala S. S., 2011, *MNRAS*, 415, 3798
- Kewley L. J., Dopita M. A., Sutherland R. S., Heisler C. A., Trevena J., 2001, *ApJ*, 556, 121
- Kharb P., O'Dea C. P., Baum S. A., Colbert E. J. M., Xu C., 2006, *ApJ*, 652, 177
- Kilborn V. A., Staveley-Smith L., Marquarding M., Webster R. L., Malin D. F., Banks G. D., Bhathal R., de Blok W. J. G., et al. 2000, *AJ*, 120, 1342
- Kormendy J., Ho L. C., 2013, *ARA&A*, 51, 511
- Lilly S. J., Carollo C. M., Pipino A., Renzini A., Peng Y., 2013, *ApJ*, 772, 119
- Lintott C., Schawinski K., Bamford S., Slosar A., Land K., Thomas D., Edmondson E., Masters K., et al. 2011, *MNRAS*, 410, 166
- Lintott C. J., Schawinski K., Slosar A., Land K., Bamford S., Thomas D., Raddick M. J., Nichol R. C., et al. 2008, *MNRAS*, 389, 1179
- Mahony E. K., Morganti R., Emonts B. H. C., Oosterloo

- T. A., Tadhunter C., 2013, *MNRAS*, 435, L58
- Mauch T., Sadler E. M., 2007, *MNRAS*, 375, 931
- Mihos J. C., 2004, *Clusters of Galaxies: Probes of Cosmological Structure and Galaxy Evolution*, p. 277
- Minchin R., Davies J., Disney M., Boyce P., Garcia D., Jordan C., Kilborn V., Lang R., et al. 2005, *ApJ*, 622, L21
- Moore B., Katz N., Lake G., Dressler A., Oemler A., 1996, *Nat*, 379, 613
- Moore B., Lake G., Katz N., 1998, *ApJ*, 495, 139
- Morganti R., Fogasy J., Paragi Z., Oosterloo T., Orienti M., 2013, *Science*, 341, 1082
- Moshir M., et al. 1990, in *IRAS Faint Source Catalogue, version 2.0 (1990) IRAS Faint Source Catalogue, version 2.0.* p. 0
- Nesvadba N. P. H., Neri R., De Breuck C., Lehnert M. D., Downes D., Walter F., Omont A., Boulanger F., et al. 2009, *MNRAS*, 395, L16
- Noeske K. G., Faber S. M., Weiner B. J., Koo D. C., Primack J. R., Dekel A., Papovich C., Conselice C. J., et al. 2007, *ApJ*, 660, L47
- Nyland K., Alatalo K., Wrobel J. M., Young L. M., Morganti R., Davis T. A., de Zeeuw P. T., Deustua S., et al. 2013, *ApJ*, 779, 173
- Oosterloo T., van Gorkom J., 2005, *A&A*, 437, L19
- Peng Y.-j., Lilly S. J., Kovač K., Bolzonella M., Pozzetti L., Renzini A., Zamorani G., Ilbert O., et al. 2010, *ApJ*, 721, 193
- Putman M. E., Peek J. E. G., Jounge M. R., 2012, *ARA&A*, 50, 491
- Rosario D. J., Santini P., Lutz D., Netzer H., Bauer F. E., Berta S., Magnelli B., Popesso P., et al. 2013, *ApJ*, 771, 63
- Sanders D. B., Soifer B. T., Elias J. H., Madore B. F., Matthews K., Neugebauer G., Scoville N. Z., 1988, *ApJ*, 325, 74
- Sarzi M., Shields J. C., Schawinski K., Jeong H., Shapiro K., Bacon R., Bureau M., Cappellari M., et al. 2010, *MNRAS*, 402, 2187
- Sault R. J., Teuben P. J., Wright M. C. H., 1995, in Shaw R. A., Payne H. E., Hayes J. J. E., eds, *Astronomical Data Analysis Software and Systems IV Vol. 77 of Astronomical Society of the Pacific Conference Series, A Retrospective View of MIRIAD*. p. 433
- Schawinski K., Khochfar S., Kaviraj S., Yi S. K., Boselli A., Barlow T., Conrow T., Forster K., et al. 2006, *Nat*, 442, 888
- Schawinski K., Lintott C., Thomas D., Sarzi M., Andreescu D., Bamford S. P., Kaviraj S., Khochfar S., et al. 2009, *MNRAS*, 396, 818
- Schawinski K., Lintott C. J., Thomas D., Kaviraj S., Viti S., Silk J., Maraston C., Sarzi M., et al. 2009, *ApJ*, 690, 1672
- Schawinski K., Thomas D., Sarzi M., Maraston C., Kaviraj S., Joo S.-J., Yi S. K., Silk J., 2007, *MNRAS*, 382, 1415
- Schawinski K., Urry C. M., Simmons B. D., Fortson L., Kaviraj S., Keel W. C., Lintott C. J., Masters K. L., Nichol R. C., Sarzi M., Skibba R., Treister E., Willett K. W., Wong O. I., Yi S. K., 2014, *MNRAS*, 440, 889
- Serra P., Oosterloo T., Morganti R., Alatalo K., Blitz L., Bois M., Bournaud F., Bureau M., et al. 2012, *MNRAS*, 422, 1835
- Stocke J. T., Keeney B. A., Lewis A. D., Epps H. W., Schild R. E., 2004, *AJ*, 127, 1336
- Strauss M. A., Weinberg D. H., Lupton R. H., Narayanan V. K., Annis J., Bernardi M., Blanton M., Burles S., et al. 2002, *AJ*, 124, 1810
- Sturm E., González-Alfonso E., Veilleux S., Fischer J., Graciá-Carpio J., Hailey-Dunsheath S., Contursi A., Poglitsch A., et al. 2011, *ApJ*, 733, L16
- Susa H., Umemura M., 2004, *ApJ*, 610, L5
- Taylor E. N., Webster R. L., 2005, *ApJ*, 634, 1067
- Tojeiro R., Masters K. L., Richards J., Percival W. J., Bamford S. P., Maraston C., Nichol R. C., Skibba R., Thomas D., 2013, *MNRAS*, 432, 359
- Verdes-Montenegro L., Sulentic J., Lisenfeld U., Leon S., Espada D., Garcia E., Sabater J., Verley S., 2005, *A&A*, 436, 443
- Verley S., Leon S., Verdes-Montenegro L., Combes F., Sabater J., Sulentic J., Bergond G., Espada D., et al. 2007, *A&A*, 472, 121
- Vollmer B., Cayatte V., Balkowski C., Duschl W. J., 2001, *ApJ*, 561, 708
- Wong O. I., Schawinski K., Kaviraj S., Masters K. L., Nichol R. C., Lintott C., Keel W. C., Darg D., et al. 2012, *MNRAS*, 420, 1684
- Wong O. I., Webster R. L., Kilborn V. A., Waugh M., Staveley-Smith L., 2009, *MNRAS*, 399, 2264
- Yi S. K., Yoon S.-J., Kaviraj S., Deharveng J.-M., Rich R. M., Salim S., Boselli A., Lee Y.-W., et al. 2005, *ApJ*, 619, L111
- York D. G., Adelman J., Anderson Jr. J. E., Anderson S. F., Annis J., Bahcall N. A., Bakken J. A., Barkhouser R., et al. 2000, *AJ*, 120, 1579
- Young L. M., Scott N., Serra P., Alatalo K., Bayet E., Blitz L., Bois M., Bournaud F., et al. 2013, *ArXiv e-prints*
- Yun M. S., Reddy N. A., Condon J. J., 2001, *ApJ*, 554, 803
- Zwaan M. A., Kuntschner H., Pracy M. B., Couch W. J., 2013, *MNRAS*, 432, 492